Ultrafast energy redistribution in C_{60} fullerenes: A real time study by two-color femtosecond spectroscopy

Ihar Shchatsinin, Tim Laarmann,[a] Nick Zhavoronkov, Claus Peter Schulz, and Ingolf V. Hertel[b]
Max Born Institute, Max-Born-Str. 2a, D-12489 Berlin-Adlershof, Germany

(Received 9 September 2008; accepted 24 October 2008; published online 26 November 2008)

Strong-field excitation and energy redistribution dynamics of C_{60} fullerenes are studied by means of time-resolved mass spectrometry in a two-color femtosecond pump-probe setup. Resonant pre-excitation of the electronic system via the first dipole-allowed HOMO$\rightarrow$LUMO+1(t_{1g}) (HOMO denotes highest occupied molecular orbital and LUMO denotes lowest unoccupied molecular orbital) transition with ultrashort 25 fs pulses at 399 nm of some 10^{12} W cm^{-2} results in a highly nonequilibrium distribution of excited electrons and vibrational modes in the neutral species. The subsequent coupling among the electronic and nuclear degrees of freedom is monitored by probing the system with time-delayed 27 fs pulses at 797 nm of some 10^{13} W cm^{-2}. Direct information on the characteristic relaxation time is derived from the analysis of transient singly and multiply charged parent and fragment ion signals as a function of pump-probe delay and laser pulse intensity. The observed relaxation times $\tau_{el} \simeq 60-400$ fs are attributed to different microcanonical ensembles prepared in the pre-excitation process and correspond to different total energy contents and energy sharing between electronic and vibrational degrees. The characteristic differences and trends allow one to extract a consistent picture for the formation dynamics of ions in different charge states and their fullerenelike fragments and give evidence to collective effects in multiple ionization such as plasmon-enhanced energy deposition. © *2008 American Institute of Physics*.
[DOI: 10.1063/1.3026734]

I. INTRODUCTION

The competition between ionization and fragmentation of polyatomic molecules interacting with intense ultrashort laser pulses is a subject of considerable current interest (see, e.g., Ref. 1). With its unique highly symmetric structure and the large number of electronic and nuclear degrees of freedom the C_{60} fullerene has proven to be a particular instructive model for studying energy deposition, redistribution, and coupling in a finite many-body system, both experimentally and theoretically (see Ref. 2, and references therein).

Of specific interest and controversy is the interplay between single active electron (SAE) response, which dominates the strong-field interaction with atoms,[3,4] and nonadiabatic multielectron dynamics (NMED) expected in complex systems.[5–10] SAE is assumed to be predominant for very short pulses as it reflects the simple fact that the fundamental interaction of photons with a many-electron system is given by an independent sum of one-electron dipole interactions, while NMED is mediated by electron correlations which require, in addition to a sufficient number of electrons, also an electron-photon interaction time at least comparable to the electron-electron interaction time which is considered to be approximately 50–100 fs. Of similar interest is the role of intermediate electronically excited states in the absorption process[11–13] and efficient coupling of electronic to nuclear motion.[14–19] Related to these "hot topics" in current femtosecond laser-based research on isolated fullerenes is the investigation of characteristic coupling times for the energy flow within the electronic system and into nuclear degrees of freedom. One may speculate that for C_{60} with its 240 valence electrons and 174 vibrational degrees of freedom, models used in metal or semiconductor physics might give some useful insights into the time scales relevant for energy redistribution in C_{60}: we argue that *molecular physics meets solid state physics* when studying strong-field effects induced in this special hollow semiconductor nanosphere. In classical Fermi liquid theory (FLT), electron-electron collision time is $\tau_{el} \propto (E-E_F)^{-2}$, where $E-E_F$ is the excess electron energy above the Fermi level E_F. In reality τ_{el} depends on the type of system and its dimensionality. Just to give an idea on the order of magnitude involved here, we refer to an experimental 2-photon photoelectron emission study for single walled carbon nanotubes[20] (a system which certainly bears some resemblance to C_{60}). There, an empirical relation for the electron coupling time $\tau_{el}/\text{fs} \simeq 30[(E-E_F)/\text{eV}+4]^{-1.5}$ was derived, corresponding, e.g., for $(E-E_F) \simeq 0.66$ eV to 60 fs, while for $E-E_F \simeq 0.03$ eV a relaxation time of $\simeq 250$ fs was found. However, these models and numbers are certainly not directly applicable to our present system. We have to keep in mind that C_{60} is a large but still finite molecular system with discrete energy levels and well-defined modes of nuclear motion. Parameters such as "electron temperature" or "back-

[a]Present address: HASYLAB at DESY, Notkestr. 85, 22607 Hamburg, Germany.
[b]Electronic mail: hertel@mbi-berlin.de. Also at Department of Physics, Freie Universität Berlin, Arnimallee 14, 14195 Berlin, Germany.

bone temperature" have to be taken with a grain of salt when describing the photophysical and photochemical processes encountered here. In particular, one would rather tend not to attribute relaxation times τ_{el} experimentally observed to electron-electron coupling exclusively. Rather, highly excited electrons formed during an intense laser pulse will exchange energy by the combined action of electron-electron scattering and electron coupling with the various nuclear degrees of freedom of the neutral molecule. In a solid state language one might say that one highly excited electron-hole pair may create several medium excited ones, all of which may couple to the nuclear backbone by electron-phonon scattering. In molecular language this would correspond to internal conversion (IC) of superexcited states involving vibrational energy population according to Franck–Condon (FC) factors.

In the past work on the interaction of ultrafast, intense laser pulses with C_{60} two key parameters were identified: laser pulse intensity and laser pulse duration determine the energetics and dynamics of ionization and fragmentation. Essentially three different ionization regimes can be distinguished, which depend sensitively on the excitation time scale.[9,21] For very short pulses (FWHM $<$ 70 fs) (FWHM denotes full width at half maximum) the excitation energy tends to remain mainly in the electronic systems and multiply charged C_{60}^{q+} ions are observed, formed by direct multiphoton ionization (MPI), possibly enhanced by transient, quasiresonant multiphoton excitation[9] of the plasmon resonance[22] between 10 and 28 eV. Relatively few fullerenelike fragments C_{60-2m}^{q+} are generated and detected in typical mass spectra under these conditions. For longer pulses (70 fs $<\tau<$ picoseconds) the absorbed energy is efficiently coupled among electronic degrees of freedom, and any fingerprints for a clear SAE ionization mechanism, such as above threshold ionization (ATI), disappear.[21] For still longer pulses ($\tau >$ picoseconds), electron-electron and electron-phonon couplings lead to substantial excess vibrational energy in the system, multiply charged ions disappear from the mass spectra, and massive fragmentation into singly charged fullerenelike species with $m \lesssim 10$, as well as into small fragments C_k^+ with $k \lesssim 27$, are observed, resulting in the well known bimodal mass distribution. In addition, delayed ionization sets in.[23]

In the present work we report on a systematic two-color pump-probe mass-spectrometric study of the characteristic time scales involved in the ionization and fragmentation dynamics of C_{60} fullerenes. The basic idea is to mimic the effect of elongated pulses by a femtosecond pump-probe approach with variable time delay between the pulses. The excitation and subsequent relaxation cascade addressed are depicted in Fig. 1. A relatively weak first 399 nm pulse deposits (pumps) energy into the electronic and vibrational system which leads to a highly excited, nonequilibrium population of states without significantly ionizing the system. Energy redistribution, i.e., "cooling" within the electronic system and coupling this energy into the nuclear degrees of freedom of the neutral system is then monitored (probed) by a delayed 797 nm pulse. Inelastic electron-electron scattering and electron-phonon coupling are thought to occur on time scales τ_{el} from some tens to some hundreds of femtoseconds.[21,24] In

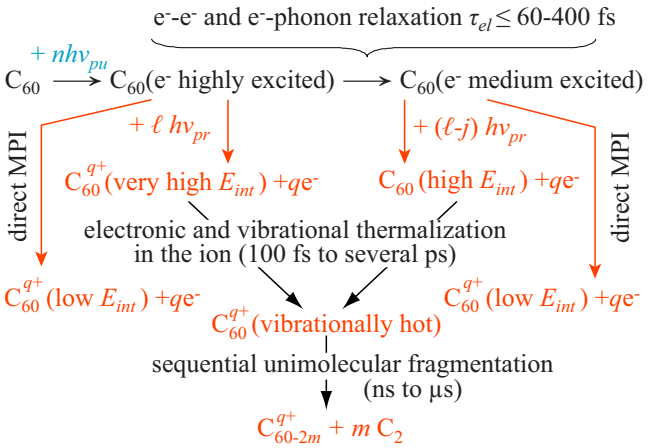

FIG. 1. (Color online) Illustration of energy redistribution processes in laser-excited C_{60} fullerenes monitored in the present work with two-color pump-probe spectroscopy (for details see text).

previous studies such information was extracted rather *indirectly* from pulse duration dependent experiments. In contrast, femtosecond pump-probe techniques offer a more *direct* view into the dynamics with a temporal resolution of nuclear motion by comparing the time-dependent signals of parent C_{60}^{q+} and fragment C_{60-2m}^{q+} ions (transients). As schematically indicated in Fig. 1, these ions are generated by the red probe pulse via direct MPI (i.e., immediately) or, respectively, after sequential evaporation of C_2 molecules on a time scale of nanoseconds to several microseconds.

We recall that the wavelength of blue, frequency doubled Ti:sapphire laser pulses (~400 nm or 3.1 eV) nearly coincides with a first small maximum in the optical absorption spectrum of neutral C_{60} which can be attributed to the first dipole-allowed HOMO(h_u) $\rightarrow$ LUMO+1(t_{1g}) (HOMO denotes highest occupied molecular orbital and LUMO denotes lowest unoccupied molecular orbital) transition.[25] (We note that this value for the excitation energy was also verified in the theoretical work of Bauer *et al.*[6] on C_{60} in strong laser fields, based on a jellium type dynamical model; we mention, however, that theoretical studies often use slightly different excitation energies, consistent with the simplified, e.g., Hückel-type energy calculations for the t_{1g} orbital.)

It is interesting to note that the population of this molecular state has also been identified to play a key role in the excitation of C_{60} Rydberg states.[26] It should be pointed out that the intensity of the blue pump pulse used throughout this study (we call it relatively weak) is still many orders of magnitude higher than that typically used in linear absorption spectroscopy: high enough to deposit several photons quasi resonantly into the system, but still weak enough to keep MPI (much smaller cross section) by the blue photons essentially negligible.

The interpretation of the present experimental data has benefited from recent theoretical work on C_{60} interaction with intense, short laser pulses tuned into resonance with this transition. Using a time-dependent density matrix formalism Zhang *et al.*[7] studied the interaction for a pulse duration of 10 fs and a laser intensity of 3×10^{10} W cm^{-2}. Although this does not exactly match our present experimental conditions,

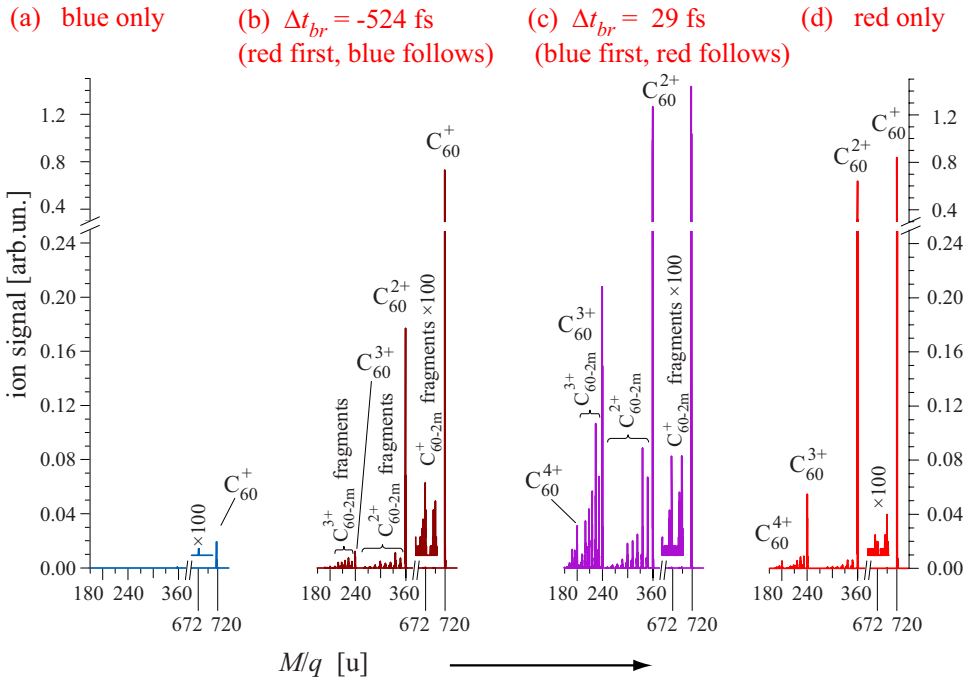

FIG. 2. (Color online) Mass spectra [ion yield as a function of mass/charge ratio (M/q) in u] after C_{60} interaction with blue (399 nm, 3.4×10^{12} W cm^{-2}) and/or red (797 nm, 5.1×10^{13} W cm^{-2}) laser pulses. (a) Only the blue pulse is active; (b) the red pulse leads, blue follows, Δt_{br}=−524 fs; (c) blue pulse leads (pump), red follows (probe), Δt_{br}=29 fs corresponding to maximum signal; and (d) only the red pulse is active. Note the break in the ion signal scale between 0.18 and 0.2 arbitrary units, followed by different scalings. Similarly the mass scale is broken between M/q=380 u and 650 u. The small insets for the C_{60-2m}^{+} fragments illustrate that these signals are extremely weak.

the calculations have revealed some interesting general trends pertinent to the present work. They predict that the initial electronic configuration of C_{60} is significantly changed upon laser irradiation. Even at these low intensities and extremely short interaction times already two electrons are excited to the LUMO+1 orbital during the femtosecond laser pulse. Due to strong coupling between the backbone and the electronic system, this is associated with an oscillatory exchange between electronic and vibrational motion of almost 2 eV. More recently, they also demonstrated efficient electron-electron correlation upon ultrafast near-resonance excitation.[13]

The theoretical work of Laarmann *et al.*[18] combines time-dependent density functional theory with classical molecular dynamics (MD) in the so-called nonadiabatic quantum MD approach.[27] Intensities up to 6×10^{13} W cm^{-2} are modeled for pulses of 27 fs duration, as in our present experiment. For the highest intensities they found that an energy equivalent of 160 blue laser photons may be absorbed during the laser pulse which is stored in about 30 excited electrons. They found the corresponding electronic energy to be strongly coupled to the $a_g(1)$ vibrational mode, leading to dramatic oscillation amplitudes: the molecule expands up to 9.4 Å, corresponding to 130% of the equilibrium C_{60} diameter! The electronic energy acquired by the system is found to be damped with time constants of ~50–150 fs, obviously due to coupling with various degrees of freedom for electronic and nuclear motion. It must be pointed out, however, that this oscillation manifest themselves in our pump-probe experiment only in spurious wiggles on the main features but can be amplified in an optimal control experiment when maximizing the energy deposition into nuclear motion by judiciously chosen pulse shapes.[18] Obviously, the theoretical model calculations underestimate the dephasing due to electron-electron and electron-vibrational couplings as a consequence of simplifying the complexities in describing the interaction between 240 valence electrons and 174 vibrational degrees of freedom.

Finally, a very interesting result of the jellium type calculations by Bauer *et al.*[6] is revealed by Fourier analysis of the calculated dipole oscillations of the system. It turns out that *after* the interaction with an intense laser pulse at 800 nm or 1.56 eV (2-photon resonant) the second harmonics of the corresponding frequency is the most prominent oscillation in the system, documenting the dominant role of this particular LUMO+1(t_{1g}) state in the strong laser field induced excitation process.

Generally speaking, the LUMO+1(t_{1g}) can act as a "doorway" state[28] accessible by a dipole-allowed transition at ~400 nm. Hence, the blue pulse—even if not yet intense enough to ionize the system—can act very efficiently as a pump to populate this state and distort the electronic structure (dynamic Stark effect[37]) sufficiently to smear out the vibrational structure and to overcome a crucial bottleneck beyond which efficient deposition of more photons becomes easy. Thus, using ultrashort "blue" pulses for quasiresonant dipole excitation of the t_{1g} orbital and intense "red" pulses for probing (by ionizing and fragmenting the system) allows one to investigate the role of intermediate excited states for energy deposition and redistribution. The present work provides a systematic study of these processes, monitored by the transient signals for a range of ionic charge states and fullerenelike fragment ions.

This paper is organized as follows. In Sec. II we describe some experimental details of the two-color pump-probe setup and the time-of-flight mass spectrometer used for time-resolved ion detection. In Sec. III results are evaluated and discussed in terms of characteristic time scales, Sec. IV gives a short summary, and in the Appendix we describe the fitting procedure used to evaluate the measured transients.

II. EXPERIMENT

The time-resolved mass-spectrometric study is based on a standard pump-probe scheme making use of a reflectron time-of-flight (ReTOF) mass spectrometer and a commercial laser system. The mode-locked Ti:sapphire femtosecond laser consists of an oscillator (Femtosource Scientific PRO, Femtolasers) pumped by a 5 W Nd:YAG (yttrium aluminum garnet) laser (Millennia V, Spectra-Physics) and a multipass amplifier (Femtosource Omega PRO, Femtolasers) pumped by a 9 W Nd:YLF (yttrium lithium fluoride) laser (YLF621D, B. M. Industries). It delivers 797 nm pulses of $t_{1/2}^{(r)}=27$ fs duration with a bandwidth of 45 nm (FWHM) at 1 kHz repetition rate. The laser pulse duration is given here at FWHM. For convenience of writing, we will also refer to the $1/e$ time τ of the pulse intensity as described in the Appendix. The maximum available pulse energy is about 800 μJ.

The output laser beam is split into two parts (1:4) by a 1 mm beam splitter in order to generate synchronized pulses. The first part is passed through a motorized translation stage controlled by a LABVIEW-PC, which sets the time delay between the pump and probe pulses. The second part is sent through a telescope to reduce the beam size and to generate second harmonic radiation in a type-I phase matching nonlinear β-barium-borate crystal of 100 μm thickness. The center wavelength of the second harmonic pulses of 25 fs duration is 399 nm with a spectral bandwidth of 11 nm (FWHM). The pulse duration is measured by means of frequency-resolved optical gating.[29] For altering the intensity of the pump and probe pulses two graded, metallic neutral density reflection filters (NDS-25C-2, Thorlabs) are used. The reflectivity of the filter can be changed in the range from 7% to 90%. The Gaussian laser beams are focused with two separate concave spherical mirrors (blue, $f=150$ cm and red, $f=100$ cm) onto the C_{60} molecular beam resulting in a beam waist (radius at $1/e$ of the maximum intensity) of 70 and 40 μm, respectively. The focal spot is characterized by imaging the attenuated laser beams on a charge coupled device camera. The maximum peak intensity reached in the experiments is 1.9×10^{13} W cm^{-2} for the blue and 7.6×10^{13} W cm^{-2} for the red pulses. A dichroic beam splitter is placed in front of the vacuum chamber to overlap the pump and the probe beam in space and to assure collinear propagation through the interaction region. The laser polarization vectors of both beams are aligned perpendicular with respect to each other. The dispersion introduced by the thin (250 μm) entrance window of the apparatus is negligible for the pulse duration used in these experiments.

The C_{60} molecular beam is produced by evaporation of gold grade C_{60} powder in an oven heated to 775 K. The laser beams are focused perpendicular to both, the effusive molecular beam and the spectrometer axis. The ions created in the intersection volume are extracted by a static electric field (Wiley–McLaren configuration), directed by the ReTOF mass spectrometer onto multichannel plates, and finally counted after amplification and discrimination by a multiscaler card (P7886, FAST ComTec). A detailed description of the ReTOF including voltage settings is given in a previous paper.[12] Typically, full mass spectra are accumulated over

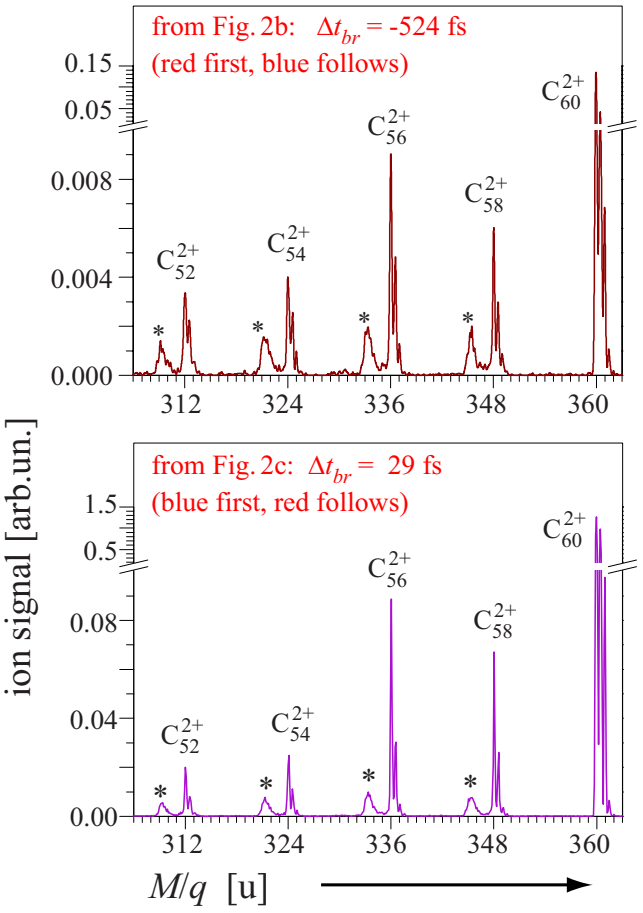

FIG. 3. (Color online) Expanded M/q scale for a section of the mass spectra in Figs. 2(b) and 2(c) illustrating the mass resolution and showing metastable decay (peaks marked by $*$) into fullerenelike fragments C_{60-m}^{2+}. Otherwise as Fig. 2. Note again the break in the ion signal scales and the different scales. The ion yields for $\Delta t_{br}=29$ fs are approximately ten times larger than for $\Delta t_{br}=-524$ fs!

5000 laser shots for each time delay Δt_{br} between the blue and red laser pulses. Examples are given in Figs. 2(a)–2(d). The mass resolution is $\simeq$0.5 u at $M/q=700$—sufficient to resolve the isotope distribution of carbon atoms in C_{60}^{q+} ions and their fragments. This is exemplified in Fig. 3, where on an enlarged mass scale a section of the mass spectra is shown (doubly charged parent and fragment ions C_{58}^{2+} to C_{52}^{2+}). As also documented there, a detailed inspection of the mass spectra shows that all fullerenelike fragments have a small satellite peak on their lower M/q side. These so-called metastable peaks (marked by "$*$") arise from fragmentation in the field-free region of the ReTOF during some tens of microseconds.

The mass spectra are taken at varying delay times Δt_{br} ranging from −530 to 530 fs in step sizes of 6.7 fs. From these, transient ion signals are derived by integration over the full area of the individual mass peaks for parent C_{60}^{q+} and fragment C_{60-2m}^{q+} ions (including the metastable peaks) of charge states $1\leq q\leq 4$ (for parents even up to 5). For positive Δt_{br} the blue pump pulse leads, the red probe pulse follows—and vice versa for negative delays. The pump-probe scans are repeated at least five times in order to achieve good statistics. "Red only" and "blue only" mass spectra are recorded before and after each scan. The stability

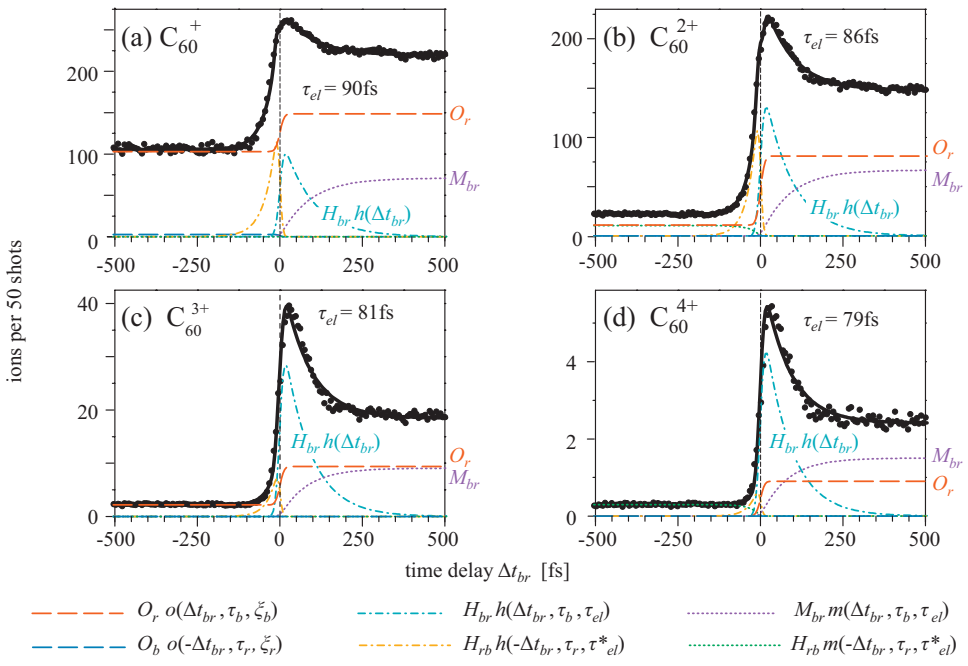

FIG. 4. (Color) Total ion yield for different charge states C_{60}^{q+} as function of the time-delay between 399 nm pump (3.4×10^{12} W cm^{-2}) and 797 nm probe pulse (5.1×10^{13} W cm^{-2}). At positive delay times the blue pulse comes first, the red follows, while the opposite holds for negative delay times. Zero delay, determined from MPI in Xe (see text), is indicated by the vertical black dashed line. The transient ion signals are fitted (full black line) with individual contributions indicated in the legend and described in the Appendix.

of the laser pulse energy during the experiment is routinely monitored with a fast photodiode. Small traces of Xe (1.0×10^{-6} mbar) are continuously added to the recipient for two reasons: (i) to precisely determine zero delay between pump and probe pulses by measuring the Xe^+ cross-correlation signal via MPI from Xe atoms (its FWHM being $t_{1/2}=45\pm3$ fs) and (ii) to find the optimum spatial overlap between pump and probe pulses by maximizing the Xe^+ ion yield at zero time delay.

III. RESULTS AND DISCUSSION

Figures 2(b) and 2(c) compare typical mass spectra resulting from the interaction of C_{60} with the combined blue and red laser pulses with those obtained from only the blue (a) or only the red (d) laser pulse. The intensity of the blue laser pulse is here chosen such that the ion signal is nearly vanishing: only a very weak C_{60}^+ signal (notice the scale breaks) is seen in Fig. 2(a). In contrast, C_{60} interaction with only the significantly more intense red laser pulse leads already to substantial ion signals, dominated by unfragmented (parent) C_{60}^{q+} ($q=1-4$) ions, as documented in Fig. 2(d). The pattern changes significantly when red and blue pulses are combined. If the red pulse hits the C_{60} prior to the blue pulse, the parent signals decrease in favor of the smaller, fullerenelike fragments down to C_{44}^{q+} (for $q\geq2$), i.e., ion fragmentation is clearly enhanced by the additional blue pulse [cf. Fig. 2(d) with Fig. 2(b)]. The most dramatic change in the mass spectra is detected, however, when the blue (pump) pulse comes first: all parent ions are significantly enhanced and the fragment C_{60-2m}^{q+} signals increase by a factor of up to 15 (with $m=1-6$ clearly visible for $2\leq q\leq4$). Note that in all cases the fragment signals of singly charged C_{60}^+ ions are extremely weak, as indicated by the small insets (signal multiplied by a factor of 100).

To follow the temporal behavior of the transient ion signals in detail, Fig. 4 shows the parent ion C_{60}^{q+} ($q=1-4$) signals as a function of time delay Δt_{br} between the 399 nm pump and 797 nm probe pulse. Figure 5 reports the analogous transients for some selected fullerenelike fragments C_{60-2m}^{3+} ($m=2,4,6$) in comparison with their parent C_{60}^{3+}. As already mentioned, the blue only signal (relatively weak pulse intensity of 3.4×10^{12} W cm^{-2}) is nearly negligible, as indicated by the height of the navy-blue long dashed lines. Only for C_{60}^+ shown in Fig. 4(a) it can be distinguished from zero for $\Delta t_{br}\ll0$. In contrast, the red only signal (pulse intensity of 5.1×10^{13} W cm^{-2}) is substantial as we have already seen in the mass spectrum in Fig. 2(d). We have indicated this in Figs. 4 and 5 by the height of the red long dashed lines for $\Delta t_{br}\gg0$ marked as O_r.

As discussed in Sec. I, quasiresonant excitation of the doorway state associated with the t_{1g} by the blue pulse leads to the absorption of several blue photons. Much higher intensities are needed to achieve the same effect by a red laser pulse only since at this photon energy one can access the same energetic region only by a (much weaker) 2-photon process. Consequently, the key observation documented in Figs. 4 and 5 is a significant enhancement of all ion signals upon pre-excitation of the neutral C_{60} molecule by the blue, quasiresonant laser pulse. The signals reach a maximum at around 30–70 fs, beyond which they decay with a lifetime of $\simeq$60–200 fs to a level still significantly above the red only signal. For even longer delay times (not shown here) the parent ion yields stay essentially constant at least up to 10 ps, while the fullerenelike fragments show a slight tendency to further decrease with Δt_{br} during this time interval (to not less than $\simeq$80% of the signal at 500 fs). This is in agreement with our own earlier observations in the context of exciting Rydberg states[26] as well as with lifetime measurements of C_{60} at much lower intensities and temperatures in cryogenic matrices.[30]

Guided by the process scheme in Fig. 1 we rationalize the observed transients for the combined action of the weak blue and strong red pulses by *essentially three effects* on the

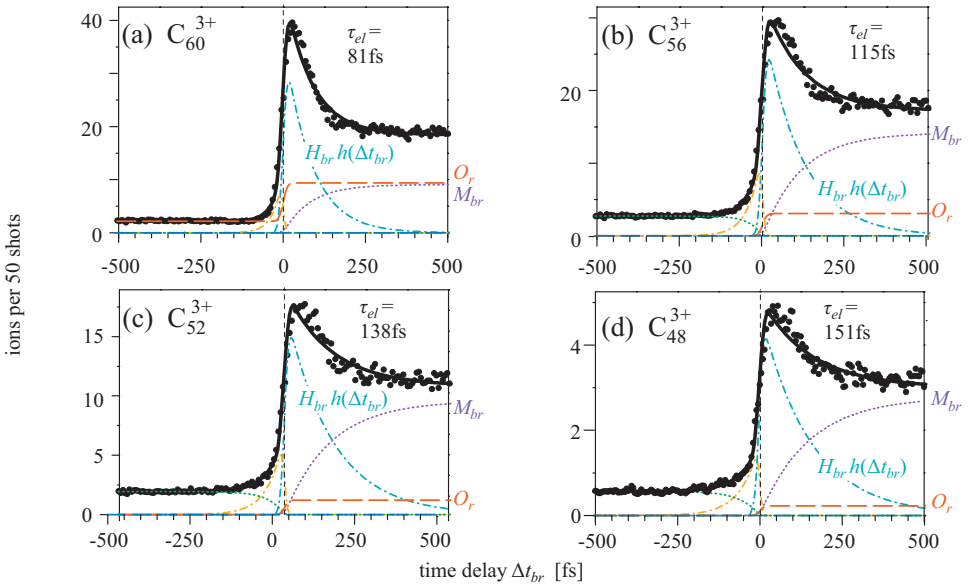

FIG. 5. (Color) Total ion yield for different fragments C_{60-2m}^{3+} as function of the time delay between 399 nm pump and 797 nm probe pulse. Otherwise as Fig. 4.

formation dynamics of parent and fullerenelike fragment ions.

(1) As we have seen, the red probe pulse only can already create significant ion signals directly out of the neutral ground state of the system; however, if the blue pulse follows ($\Delta t_{br}<0$), it reduces the ion signals due to excitation of these ions, thus initiating subsequent ion fragmentation on the nanosecond and microsecond time scale (a process differing in significance from ion to ion).

(2) Several blue pump pulse photons can be absorbed and may generate highly excited electrons—which do, however, not yet ionize. They thermalize rapidly through inelastic scattering among the electronic degrees of freedom and coupling to the nuclear motion on a time scale τ_{el} (the relaxation time of the respective highly excited neutral parent); when the red probe pulse follows the blue ($\Delta t_{br}>0$), the system is ionized from highly excited states particularly efficiently (larger transition-dipole moments and/or FC factors). The ion yields hence increase dramatically and maximum ionization is found at $\Delta t_{br}\simeq 30-70$ fs.

(3) With the same time constant τ_{el} a thermalized (medium hot) electron population builds up and can also be ionized by the red probe pulse for $\Delta t_{br}>0$. In contrast to the highly excited state, the ionization probability is somewhat lower for these medium energy electrons (still higher though than for direct ionization from the ground state). For $\Delta t_{br}\gtrsim 200$ fs (up to at least some picoseconds) the ion signals remain essentially constant or decrease only very slowly.

Efficient population of the LUMO+1(t_{1g}) doorway state is obviously a rate limiting step for depositing energy into the system. A laser pulse of relatively moderate intensity can initiate multielectron excitation when tuned into resonance, as first modeled by Zhang and co-workers.[7,31] Also, we will later present some evidence that even immediately after the pump pulse vibrational energy is already excited: the initial energy deposition is shared between electronic and nuclear degrees of freedom. This all dramatically facilitates ionization and additional energy deposition by the red probe pulse which finally leads to a vibrationally hot ionic system that readily fragments on a nanosecond or microsecond time scale.

In this context, another interesting quantity to study as a function of delay time Δt_{br} is the relative abundance of metastable fullerenelike fragments which can be derived from the metastable peaks indicated by $*$ in Fig. 3. Two examples which show a particular clear trend are given in Fig. 6. We have refrained here from a more sophisticated fit. However, we clearly see a significant drop in the metastable fraction as Δt_{br} changes from negative to positive, i.e., as the blue pulse pre-excites the system. This relative decrease in metastable fragments corresponds to an increase in the temperature of the system after energy equilibration and hence corroborates

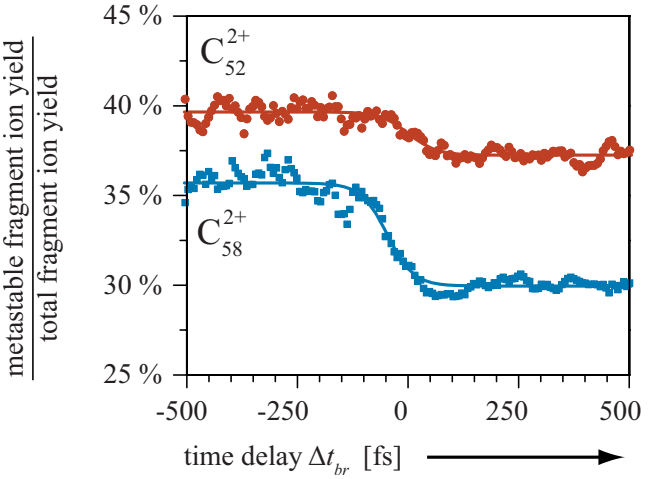

FIG. 6. (Color online) Relative yield of metastable fragment ions for the doubly charged fragments C_{58}^{2+} and C_{52}^{2+} as function of delay time, as derived from data illustrated in Fig. 3. Here, all measured signals have been smoothed over five Δt_{br} data points in order to reduce statistical noise. The lines are simple sigmoidal fits to guide the eyes.

the conclusion that the relatively weak pre-excitation leads to an significant increase in the average energy content of the system.

In the following we focus on the dynamic behavior for positive time delays $\Delta t_{br} > 0$, where it is indeed the blue pulse that selectively excites the electronic system and the strong red probe pulse causes ionization and fragmentation. Consequently, the time evolution of the *energy redistribution* process in the electronic system of the *neutral molecular* system is directly monitored by the recorded ion yields. Obviously, the cross section for subsequent multiphoton absorption of red probe photons, which finally leads to the observed distribution of parent and fragment ions, depends sensitively on the density of the excited "electron-hole plasma" as well as on the maximum energy available in the system excited by multiple absorption of blue pump photons.

For a quantitative comparison of the observed transients we have used a fit-function essentially consisting of three components corresponding to the effects discussed above,

$$f(\Delta t_{br}) = O_r o(\Delta t_{br}) + H_{br} h(\Delta t_{br}) + M_{br} m(\Delta t_{br}). \quad (1)$$

Here $O_r o(\Delta t_{br})$ describes the red only signal (for $\Delta t_{br} > 0$) and what remains of it after interaction with the blue pulse (for $\Delta t_{br} < 0$), $H_{br} h(\Delta t_{br})$ mimics the contribution from highly excited electrons to the transient ion signal (peaking at $\Delta t_{br} \simeq 30-70$ fs), and $M_{br} m(\Delta t_{br})$ corresponds to thermalized medium energy electrons (remaining constant for $\Delta t_{br} > 200$ fs). The crucial parameters to be discussed are τ_{el} and the ratio H_{br}/M_{br}.

We find, however, that for $\Delta t_{br} \leq 0$ the experimentally determined transients (as shown in Figs. 4 and 5) can only be fitted with sufficient accuracy corresponding to the statistics of the data by also allowing for equivalent processes where the role of pump and probe pulse is exchanged, i.e., the red pulse acts as pump and the blue pulse as probe. Even though these contributions are much weaker compared to those discussed before, they are statistically significant. Nevertheless, we refrain from the temptation to interpret additional physics into the corresponding—somewhat ambivalent—fit parameters. Details of the fitting procedure are described in the Appendix. The six individual contributions are shown in Figs. 4 and 5 and those from red pump and blue probe are indeed very small. Note, in particular, that $O_b o(-\Delta t_{br}, \tau_r, \xi_r)$ describing the blue only background and its modification due to the following red pulse is almost identical to zero in all cases.

We summarize the results obtained from these fits to the parent and of fullerenelike fragment ions in Figs. 7 and 8. Unfortunately, the limited laser pulse intensity and nonlinear conversion efficiency from red to blue do not allow for much flexibility in choosing these intensities. Nevertheless, the parameters derived from two quite different sets of pump and probe pulse intensities corroborate the observations and show interesting trends from which important insights into the dynamics may be gleaned. The first set of measurements (for which details have been shown in Figs. 2–5) refers to maximum laser pulse intensities $I_{\mathrm{blue}} = 3.4 \times 10^{12}$ W cm^{-2} and $I_{\mathrm{red}} = 5.1 \times 10^{13}$ W cm^{-2}. Under these conditions the blue only signal was practically zero, while the red only signal

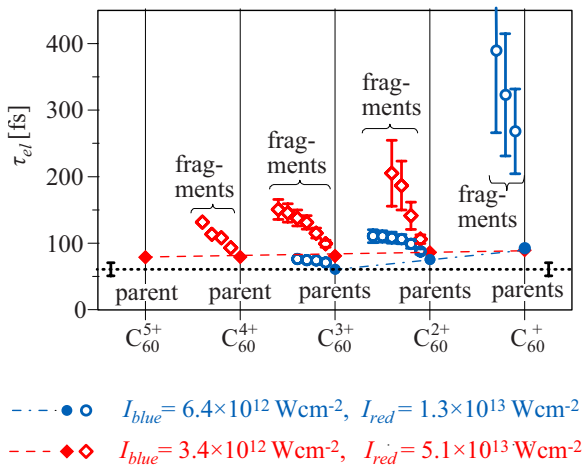

FIG. 7. (Color online) Relaxation times τ_{el} for highly excited electrons due to electron-electron and electron-vibratonal couplings as determined from fitting the transient signals shown in Figs. 4 and 5. The results are presented in this graph in analogy to the mass spectra in Fig. 2, i.e., τ_{el} for fragments C_{60-2m}^{q+} (open symbols) are ordered from $m=1-6$ to the left side of the respective parents C_{60}^{q+} (full symbols). Two sets of data for different pump and probe pulse intensities (I_{blue} and I_{red}, respectively) have been evaluated as noted in the legend. The dotted line (with error bar) indicates the electronic relaxation time for C_{60} derived in previous studies (see text), while the dashed and dash-dotted lines are drawn to guide the eyes. Note that the values of τ_{el} derived from the transients of different photoions C_{60}^{q+} and fullerenelike fragments C_{60-2m}^{q+} refer to the respective *neutral precursor* molecules.

was quite substantial, as discussed above. The second set of parameters was derived for $I_{\mathrm{blue}} = 6.4 \times 10^{12}$ W cm^{-2} and $I_{\mathrm{red}} = 1.3 \times 10^{13}$ W cm^{-2}. At these conditions, the blue only signals were still small but not negligible, while no red only signals were observed (not shown here).

For understanding these experimental results we recall the theoretical model calculations described in Sec. I. Although all of them have some characteristic shortcomings owing to the complexity of the problem, three undebatable messages may be extracted: (i) the LUMO+1(t_{1g}) state plays a key role as doorway state; (ii) following this resonant step, multielectron dynamics allows for the deposition of substantial additional energy into the system, in the present case by absorption of several blue photons; (iii) this electronic energy is strongly coupled to the nuclear motion of the system and decays on a time scale of some 10 to some 100 fs in favor of vibrational population by electron-electron and electron-phonon couplings; (iv) we have to add that on a still longer time scale (picoseconds) finally intramolecular vibrational energy redistribution among the 174 degrees of freedom fully thermalize the system, as indeed indicated by a slight decay of fragment ion signals, when the system is probed on the 1–10 ps time scale.

Thus, the clearly most significant parameter that can be derived from our present measurements is the characteristic electron relaxation time τ_{el} in the neutral C_{60} precursor molecules which are ionized by the red probe pulse. The results are summarized in Fig. 7 for the various parent and fragment ions of different charge states. The dotted line represents previous, independent determinations of τ_{el}: Campbell and co-workers[21,24] estimated about 70 fs from the disappearance of the structure in the ATI spectra associated with the C_{60}^{+}

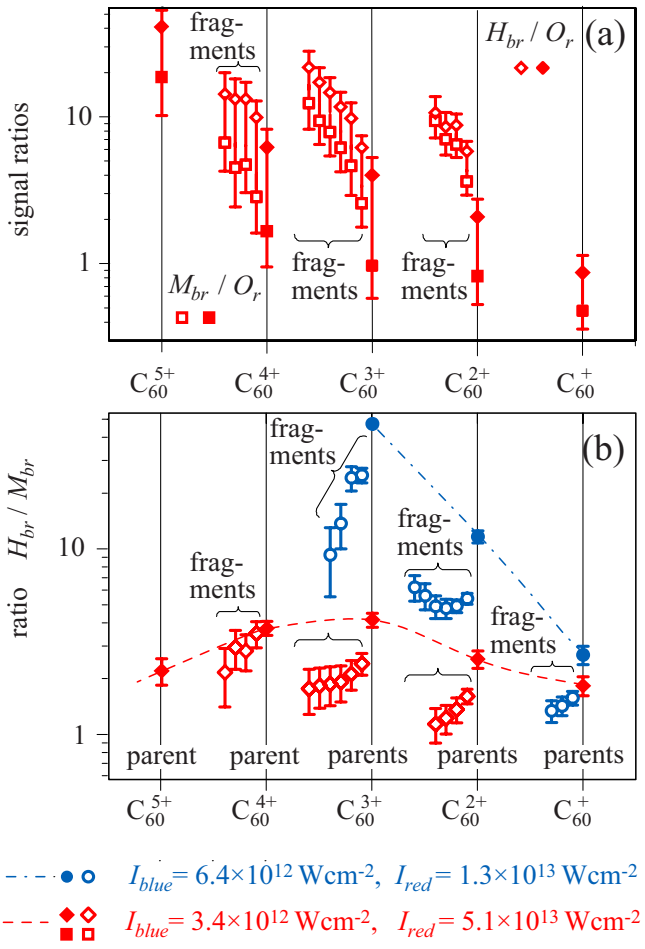

FIG. 8. (Color online) (a) Ratios H_{br}/O_r and M_{br}/O_r of *additional* ion yields from highly excited ($\propto H_{br}$) and thermalized ($\propto H_{br}$) medium energy electrons to the red only signal ($\propto O_r$) according to the scheme in Fig. 1 as derived from Figs. 4 and 5. These ratios can only be given for the more intense red laser pulse since with the weaker red laser pulse the red only signal O_r vanishes. (b) Ratios H_{br}/M_{br} of ion yields from highly excited to those from thermalized, medium energy electrons. Otherwise as Fig. 7.

formation, while we recently[9] obtained $\tau_{el} \simeq 50$ fs in a one-color pump-probe experiment with extremely short, intense red pulses (FWHM=9 fs, 7.9×10^{13} W cm^{-2}) detecting C_{60}^{+}. Obviously, the measurements do not refer to exactly identical conditions but still agree rather well.

To understand the trends documented in Fig. 7 we refer to the relation between excess electron energy and electron-electron collision time in the FLT model as well as to the empirical numbers for single walled carbon nanotubes, briefly discussed in Sec. I. Although certainly not directly applicable to free C_{60} molecules, we expect that the general trend found there should also hold for our relaxation time τ_{el}: *the higher the excess electron energy, the faster the relaxation of very highly excited electrons*. Equivalently, in a molecular picture one would argue that IC occurs with the highest rate for highly excited states where the density of acceptor states is largest.

In order to connect this general wisdom with the observed trends shown in Fig. 7, we have to remember some important facts about ionization and fragmentation of a large finite system such as C_{60}.

- While ionization occurs instantly after absorption of an appropriate number of probe photons, large fullerene fragments are generated from hot C_{60}^{q+} by sequential evaporation of C_2 units on a time scale of nanoseconds to microseconds, i.e., a very long time after blue and red femtosecond-laser pulses have interacted with the system. The fragmentation patterns are just a signature of the internal energy deposition and redistribution initiated by the femtosecond-laser pulses. We could say that the fragmentation acts as thermometer for the primary process which ends after some picoseconds.
- The total energy needed to generate the different parent and fragment ions differs vastly;[32,33] e.g., for simply ionizing C_{60} molecules by red laser pulses one needs, in principle, only 5 photons (7.56 eV) (with a probability for direct MPI depending on the fifth power of the red photon intensity); in contrast, in order to allow a fullerenelike fragment such as C_{48}^{4+} to be formed, at least 60 eV are required for ionization plus 60–70 eV for fragmentation (10–12 eV for each C_2 dissociation) and in addition an excess energy of about 30 eV, the so-called *kinetic shift* (see, e.g., Refs. 34 and 35), has to be deposited to observe the fragments on the time scale of nanoseconds to microseconds accessed by the mass spectrometer.[38] Thus, in total at least 150–160 eV internal energy is needed to observe C_{48}^{4+} which amounts to about 100 red photons being absorbed in the red only experiment. As our results document, this absorption process is apparently strongly enhanced by the resonant blue pulse pre-excitation, which prepares the neutral C_{60} molecules in a especially favorable state (from which absorption of many red photons into highly excited vibrational states of the ions may proceed).
- The thus prepared sample of excited neutral C_{60} molecules consists of a multitude of microcanonical ensembles with different total energies which initially are not in thermal equilibrium. This is not only due to the fact that the target itself is prepared in a thermal energy distribution (effusive molecular beam at several 100 K) with a broad range of absorption cross sections (see, e.g., the failure to excite Rydberg states from cold in contrast to hot C_{60} molecules as reported in Ref. 26). In addition multiphoton absorption generally will lead to a multitude of excited states with different total energies (e.g., in the Poisson distribution corresponding to a different number of absorbed photons) and due to different energy sharing between electronic and vibrational energy characterized by the respective FC factors.

Each of these microcanonical ensembles will have a specific characteristic relaxation time τ_{el} and a particular preference to finally end as a specific product, such as a parent C_{60}^{q+} or a fullerenelike fragment ion C_{60-2m}^{q+}. This is precisely what we see in Fig. 7. We consider the relaxation parameter τ_{el} to reflect the thermalization of electrons in the different microcanonical ensembles by electron-electron and electron-

phonon scatterings. Fast relaxation then corresponds to a high excess electron energy, while slower relaxation times indicate lower electron energies.

Several trends may be identified: (i) the higher the pump pulse intensity and (ii) the higher the detected charge state of parent ions $C_{60}^{q+}, q=1-5$, the faster is the relaxation process. The lowest value observed here[39] is $\tau_{el} \simeq 60$ fs for C_{60}^{3+} with $I_{blue}=6.4\times10^{12}$ W cm^{-2}, $I_{red}=1.3\times10^{13}$ W cm^{-2}. (iii) Fragments with an increasing number of evaporated C_2 units originate from microcanonical ensembles with increasing τ_{el}, i.e., from those with the smallest amount of excess electron energy. This trend is significantly less pronounced for the higher pump pulse intensity and higher charge states, i.e., for higher initial energy deposition. (iv) Singly charged fragments—if detected at all—originate from microcanonical ensembles with particularly long thermalization times. The longest relaxation time $\tau_{el} \simeq 400$ fs is observed for C_{54}^{+}. We remember that nearly no such fragments were seen in the mass in spectra Fig. 2 recorded with $I_{blue}=3.4\times10^{12}$ W cm^{-2}. At higher blue pump intensity they are just barely detectable. As a general trend, Fig. 7 documents that higher charge state fragments arise from precursor ensembles with slightly faster relaxation times. From all these observations a consistent qualitative picture emerges.

As a consequence of resonantly exciting the doorway state accompanied by level broadening and potential deformation, a wide variety of transitions become possible between the different electronic states (including those above the one associated with LUMO+1 and those below the HOMO state). These transitions occur on potential surfaces not directly accessible from the undisturbed ground state and lead to a multitude of microcanonical ensembles with different total energies (due to thermal initial conditions and different numbers of absorbed photons) and with a large manifold of differently shared electronic and vibrational energies. Due to the complexity of the multidimensional potential hypersurfaces and their landscape of FC factors this may even hold if only one or two additional blue photons are absorbed after the doorway state has been reached.

The detection process will enhance this trend: vibrationally pre-excited ensembles will have enhanced absorptions cross sections for the red photons, thus resulting in a population of ionic states with high vibrational excitation. Obviously the formation of parent ions (with charge q) requires precursors with as little vibrational energy as possible—otherwise the probability for enhanced vibrational excitation is large and the ensemble will lead predominantly to fragments. Now, those ensembles with the lowest vibrational excitation correspond to the highest electronic excitation and thus to the fastest relaxation: hence, τ_{el} is smallest for the parent ion. Also, those precursors with the highest electronic pre-excitation will lead to the highest charge states: the probability to reach the plasmon state is expected to be higher, the higher the pre-excitation.

Clearly, by the same argument we can explain the increasing relaxation time leading to smaller fragments: the corresponding precursor ensembles are born with increasing vibrationally excitation, hence with decreasing electronic excitation and thus have longer relaxation times. The trend when the blue pulse intensity is changed just emphasizes these observations: higher blue intensity corresponds to more electronic at the cost of vibrational excitation, hence faster relaxation of the precursor ensemble.

Finally, the long standing puzzle why so few singly charged fullerenelike fragments are seen finds now a plausible explanation: the very long relaxation times observed here tells us that the precursor has a particularly low electronic energy. Hence, the probability for accessing the (highly excited electronic) plasmon state by the red probe photon is particularly low. All other neutral ensembles with some excess electronic energy content just have a very high chance to be transferred through the plasmon state into multiply charged ions. Hence the low abundance of C_{60-2m}^{+} fragments: while vibrationally unexcited neutral C_{60} can be ionized directly by the red photon in a 5-photon process, molecules vibrationally pre-excited tend to end as multiply charged fragments—except for the very small number of ensembles which have high vibrational but nearly no electronic excitation.

The picture of the ionization and fragmentation processes thus developed is further corroborated by comparing also the ion yield parameters derived from the measured pump-probe transient ion signals. In Fig. 8 the relative importance of the signal enhancement due highly excited (H_{br}) and medium energy electrons (M_{br}) is documented. For ease of comparison we show in Fig. 8(a) their ratio to the red only signal (O_r). The ratio H_{br}/M_{br} is presented in Fig. 8(b). For the more intense blue pump pulse (weaker red probe pulse), only this ratio can be given since the red only signal vanishes in this case. (Note that H_{br} also determines the maximum signal at 30–70 fs time delay in Figs. 4 and 5.)

A clear message emerges. According to Fig. 8(a) the higher the precursor excitation is (leading to higher charge states and to more fragmentation), the more pronounced the enhancement of ionization and fragmentation by blue preexcitation in comparison to the red only signal also is: highly excited microcanonical ensembles obviously have a larger ionization cross section (involving possibly also higher FC factors) which enhances both fragments and parents.

Figure 8(b) shows the relative magnitude H_{br}/M_{br} of the relaxation, which is obviously higher if the initial energy and density of the excited electrons is higher, i.e., for the more intense blue pulse. If the electron energy after relaxation is essentially the same in both cases, this is immediately evident. Fragments arise again from those ensembles with a high average vibrational energy; thus there is less electronic excitation density to relax and the ratio H_{br}/M_{br} naturally becomes smaller. This supports our conclusion that fragmentation originates from species which are vibrationally excited but electronically rather cold. Hence, this amplitude ratio drops as more and more C_2 units can evaporate since they belong to an initially higher vibrational energy content.

IV. CONCLUSION

Strong-field excitation and energy redistribution dynamics in C_{60} fullerenes has been studied by time-resolved mass spectrometry in a two-color femtosecond pump-probe setup.

The role of intermediate excited states as rate limiting step for energy deposition, as well as for electron-electron and electron-vibrational relaxation in the molecular response, was addressed by resonant pre-excitation of the electronic system with 399 nm radiation via the first dipole-allowed LUMO+1(t_{1g}) state, the doorway state. Several photons may be deposited into the system during the interaction with the ultrashort blue pulses of 25 fs at an intensity of 3.1×10^{12} W cm^{-2}. This results—prior to ionization—in a highly nonequilibrium distribution of states with high internal energy, shared among electronic and nuclear degrees of freedom. Characteristic coupling times for energetic relaxation of electrons are derived by probing the initially neutral many-body system with delayed 27 fs pulses at 797 nm with 5.1×10^{13} W cm^{-2}.

Detailed information on the relaxation process is derived from the analysis of singly and multiply charged parent and fullerenelike fragment ion transients formed by the red probe pulse as function of pump-probe delay and pulse intensities. Three different trends were identified, characterized, and related to previous findings. (i) Electron relaxation times in the neutral precursor decrease with increasing charge state q of the eventually detected C_{60}^{q+} ($q=1-5$). The lowest coupling time is observed for C_{60}^{3+} with $\tau_{el}\simeq60$ fs (with a clear trend toward even shorter times for higher charge states). (ii) Fragments that have evaporated the largest number of C_2 units arise from pre-excited species showing the slowest electronic thermalization. These fullerenes are vibrationally hot but electronically rather cold. (iii) Electronic relaxation times observed in the fragment channels C_{60-2m}^{q+} increase with decreasing charge states and with increasing number of C_2 losses. This corresponds to more and more vibrational excitation at the cost of electronic excitation energy. The longest relaxation times $\simeq$400 fs are observed in the singly charged fragment ion channel. C_{60-2m}^{+} can apparently only be formed when the electron energy is particularly low—thus avoiding multiple ionization via quasiresonant MPI through the plasmon resonance.

This also solves the long standing puzzle why only spurious amounts of singly charged fullerenelike fragment ions are observed in mass spectra created by very fast laser pulses: the particularly low electronic excitation, combined with substantial vibrational excitation as intermediate neutral precursor required for the formation of C_{60-2m}^{+}, occurs only with a very low probability. Ensembles with higher electronic pre-excitation are much more abundant and lead to multiply charged ions by MPI via the plasmon resonance. On the other hand, C_{60} in its neutral ground state is readily ionized by 5-photon MPI without internal vibrational excitation (due to favorable FC factors) and can be detected with significant probability as parent C_{60}^{+} ions.

ACKNOWLEDGMENTS

This work has been supported by the Deutsche Forschungsgemeinschaft through Sonderforschungsbereich 450, TP A2.

APPENDIX: FITTING PROCEDURE

Without claiming to provide an exact description of the rather complex processes occurring under the combined action of the *blue pump and red probe pulses*, we rationalize the observations according to the scheme in Fig. 1 by *essentially three contributions* to the measured ion signals (parents as well as large fragment ions) as described in Sec. III. They are represented by three components of an overall fitting function.

(1) The first contribution $O_r o(\Delta t_{br})$ describes the "red only signal" O_r and its reduction to a fraction, say, ξ_b due to the blue pulse if it follows the red pulse, i.e., for $\Delta t_{br}<0$. While the parameter O_r can be measured directly [see Fig. 2(d)], the signal reduction ξ_b has to be extracted from the fitting procedure. Assuming Gaussian laser pulses

$$\exp(-[t/\tau]^2) \quad \text{with} \quad \tau\simeq0.6 \ \text{FWHM}, \tag{A1}$$

we expect that for $\Delta t_{br}>0$ (red follows blue) the reduction is "switched off" with the time constant $\tau=\tau_b$ of the blue laser pulse. We take this into account by the function

$$o(\Delta t_{br},\tau_b,\xi_b)=\frac{1}{2}(1-\xi_b)\mathrm{erf}\left(\frac{\Delta t_{br}}{\tau_b}\right)+\frac{1}{2}(1+\xi_b), \tag{A2}$$

which rises smoothly from ξ_b to 1 when the delay time Δt_{br} passes through zero.

(2) The second contribution $H_{br}h(\Delta t_{br})$ to the ion signal arises from the "highly excited" (neutral) electron distribution which builds up on the time scale τ_b of the blue pump pulse and decays with the electron relaxation time constant τ_{el} of the respective neutral parents. This signal is taken proportional to a convolution of the pump pulse with an exponential decay function

$$h(\Delta t_{br},\tau_b,\tau_{el})=\frac{1}{2}\exp\left(-\frac{\Delta t_{br}}{\tau_{el}}+\left[\frac{\tau_b}{2\tau_{el}}\right]^2\right)\times\left[1+\mathrm{erf}\left(\frac{\Delta t_{br}}{\tau_b}-\frac{\tau_b}{2\tau_{el}}\right)\right], \tag{A3}$$

which rises quickly from 0 (with time constant τ_b) to a maximum (up to 1 if $\tau_b\ll\tau_{el}$) and decays again (with time constant τ_{el}).

(3) The third contribution $M_{br}m(\Delta t_{br})$ arises from the "thermalized"(neutral) electron distribution which builds up with the same time constant τ_{el}. This signal will follow a convolution of the Gaussian pump pulse with a corresponding exponential rise function given by

$$m(\Delta t_{br},\tau_b,\tau_{el})=\frac{1}{2}\left[1+\mathrm{erf}\left(\frac{\Delta t_{br}}{\tau_b}\right)-h(\Delta t_{br},\tau_b,\tau_{el})\right], \tag{A4}$$

which starts from 0 at negative delay times $\Delta t_{br}\ll-\tau_b$ and reaches 1 for $\Delta t_{br}\gg\tau_{el}$.

Finally, we have to take account of the fact that the blue and red pulses act as pump and probe, respectively, only for $\Delta t_{br}>0$. In contrast, for negative delay times $\Delta t_{br}<0$, the

inverse may be of some importance: i.e., the red pulse can, in principle, act as pump, the blue as probe. Even though these contributions are smaller, it turns out that they are needed for an optimal fit of our data. By replacing in the above functions $\Delta t_{br} \rightarrow -\Delta t_{br}$ as well as the blue pulse time constant by that of the red pulse, $\tau_b \rightarrow \tau_r$, this can be taken into account. Also, the electron relaxation time constants may differ depending on whether blue or red pulses are used as pump. They are denoted by τ_{el} and τ_{el}^*, respectively. Thus, when taking account of all these effects, the overall fitting function can be written as

$$f(\Delta t_{br}) = O_r o(\Delta t_{br}, \tau_b, \xi_b) + O_b o(-\Delta t_{br}, \tau_r, \xi_r) + H_{br} h(\Delta t_{br}, \tau_b, \tau_{\mathrm{el}}) + H_{rb} h(-\Delta t_{br}, \tau_r, \tau_{\mathrm{el}}^*) + M_{br} m(\Delta t_{br}, \tau_b, \tau_{\mathrm{el}}) + M_{rb} m(-\Delta t_{br}, \tau_r, \tau_{\mathrm{el}}^*), \tag{A5}$$

where the fitting parameters ξ_b, H_{br}, and M_{br} determine the three contributions for blue pump and red probe, while ξ_r, H_{rb}, and M_{rb} determine the corresponding signals for red pump and blue probe. Here τ_b and τ_r are the Gaussian pulse durations according to Eq. (A1) of the blue and red pulses, respectively, while O_b and O_r are the experimentally determined signals produced by the blue and red pulses only and $O_b(1-\xi_r)$ and $O_r(1-\xi_b)$ describe the ion reduction due to the action of the red probe pulse and the blue probe pulse, respectively. Thus, the contributions $h(\Delta t_{br}, \tau_b, \tau_{\mathrm{el}})$ and $m(\Delta t_{br}, \tau_b, \tau_{\mathrm{el}})$ essentially describe the dynamics at positive delays times, while $h(-\Delta t_{br}, \tau_r, \tau_{\mathrm{el}}^*)$ and $m(-\Delta t_{br} t, \tau_r, \tau_{\mathrm{el}}^*)$ correspond to negative delays. According to Eq. (A1) laser pulse durations of $\tau_b = 0.6 \times 25$ fs and $\tau_r = 0.6 \times 27$ fs are used for the blue and red pulses, respectively. The quantities H_{br}, M_{br}, H_{rb}, M_{rb}, τ_{el}, and τ_{el}^*, as well as ξ_b and ξ_r are fitted to the experimental data.

One may question the use of the FWHM of the individual pump laser pulses (25 and 27 fs for blue and red, respectively) as critical laser time constant rather than the cross-correlation time. We argue that the probe process is an n-photon process (with $n \gg 1$) and hence will lead only to a small broadening of the pump pulse duration. We find indeed the best fits with this assumption and include these uncertainties into the estimated error bars of the parameters extracted.

It should be pointed out that the fitting procedure described here is, of course, by no means unique. It does not claim to give a realistic image of the very complex energy redistribution processes in the different microcanonical ensembles of C_{60} prepared by the pump pulse and the detection mechanism through the probe pulse. However, it rationalizes the experimentally observed transient data in a schematic overall manner according to the process scheme discussed in Sec. I and allows us to extract and compare quantitatively some characteristic parameters for different charge states and fragments as well as for different pump/probe conditions.

As it turns out, τ_{el}^* is found to be very similar to τ_{el} both in magnitude and trends but is determined with much less accuracy. Also, O_b and ξ_r are essentially zero and H_{rb} as well as M_{rb} are significantly smaller than H_{br} and M_{br}, respectively. Consequently, our discussion on the physics to be gleaned from these data focuses essentially on *two quantities* derived for $\Delta t_{br} \geq 0$ (i.e., for blue pump and red probe pulses): on the relaxation time τ_{el} and on the relative contribution from *highly excited* and *thermalized, medium energy* electrons, specifically on H_{br}/M_{br}.

[1] A. N. Markevitch, D. A. Romanov, S. M. Smith, and R. J. Levis, Phys. Rev. A **75**, 053402 (2007).
[2] I. V. Hertel, T. Laarmann, and C. P. Schulz, in *Advances in Atomic, Molecular, and Optical Physics*, edited by B. Bederson and H. Walter (Elsevier, Amsterdam, 2005), Vol. 50, pp. 219–286.
[3] A. Jaroń-Becker, A. Becker, and F. H. M. Faisal, Phys. Rev. Lett. **96**, 143006 (2006).
[4] A. Jaroń-Becker, A. Becker, and F. H. M. Faisal, J. Chem. Phys. **126**, 124310 (2007).
[5] B. Torralva, T. A. Niehaus, M. Elstner, S. Suhai, T. Frauenheim, and R. E. Allen, Phys. Rev. B **64**, 153105 (2001).
[6] D. Bauer, F. Ceccherini, A. Macchi, and F. Cornolti, Phys. Rev. A **64**, 063203 (2001).
[7] G. P. Zhang, X. Sun, and T. F. George, Phys. Rev. B **68**, 165410 (2003).
[8] T. Brabec, M. Côté, P. Boulanger, and L. Ramunno, Phys. Rev. Lett. **95**, 073001 (2005).
[9] I. Shchatsinin, T. Laarmann, G. Stibenz, G. Steinmeyer, A. Stalmashonak, N. Zhavoronkov, C. P. Schulz, and I. V. Hertel, J. Phys. Chem. **125**, 194320 (2006).
[10] M. Ruggenthaler, S. Popruzhenko, and D. Bauer, Phys. Rev. A **78**, 033413 (2008).
[11] G. P. Zhang, Phys. Rev. Lett. **95**, 047401 (2005).
[12] M. Boyle, T. Laarmann, K. Hoffmann, M. Hedén, E. E. B. Campbell, C. P. Schulz, and I. V. Hertel, Eur. Phys. J. D **36**, 339 (2005).
[13] G. P. Zhang and T. F. George, Phys. Rev. B **76**, 085410 (2007).
[14] M. Boyle, T. Laarmann, I. Shchatsinin, C. P. Schulz, and I. V. Hertel, J. Chem. Phys. **122**, 181103 (2005).
[15] G. P. Zhang and T. F. George, Phys. Rev. B **73**, 035422 (2006).
[16] R. Sahnoun, K. Nakai, Y. Sato, H. Kono, Y. Fujimura, and M. Tanaka, Chem. Phys. Lett. **430**, 167 (2006).
[17] R. Sahnoun, K. Nakai, Y. Sato, H. Kono, Y. Fujimura, and M. Tanaka, J. Chem. Phys. **125**, 184306 (2006).
[18] T. Laarmann, I. Shchatsinin, A. Stalmashonak, M. Boyle, N. Zhavoronkov, J. Handt, R. Schmidt, C. P. Schulz, and I. Hertel, Phys. Rev. Lett. **98**, 058302 (2007).
[19] K. Nakai, H. Kono, Y. Sato, N. Niitsu, R. Sahnoun, M. Tanaka, and Y. Fujimura, Chem. Phys. **338**, 127 (2007).
[20] T. Hertel and G. Moos, Chem. Phys. Lett. **320**, 359 (2000).
[21] E. E. B. Campbell, K. Hansen, K. Hoffmann, G. Korn, M. Tchaplyguine, M. Wittmann, and I. V. Hertel, Phys. Rev. Lett. **84**, 2128 (2000).
[22] I. V. Hertel, H. Steger, J. DeVries, B. Weisser, C. Menzel, B. Kamke, and W. Kamke, Phys. Rev. Lett. **68**, 784 (1992).
[23] E. E. B. Campbell, G. Ulmer, and I. V. Hertel, Phys. Rev. Lett. **67**, 1986 (1991).
[24] K. Hansen, K. Hoffmann, and E. E. B. Campbell, J. Chem. Phys. **119**, 2513 (2003).
[25] R. Bauernschmitt, R. Ahlrichs, F. H. Hennrich, and M. M. Kappes, J. Am. Chem. Soc. **120**, 5052 (1998).
[26] M. Boyle, M. Hedén, C. P. Schulz, E. E. B. Campbell, and I. V. Hertel, Phys. Rev. A **70**, 051201 (2004).
[27] T. Kunert and R. Schmidt, Eur. Phys. J. D **25**, 15 (2003).
[28] A. N. Markevitch, D. A. Romanov, S. M. Smith, H. B. Schlegel, M. Y. Ivanov, and R. J. Levis, Phys. Rev. A **69**, 013401 (2004).
[29] R. Trebino, K. W. DeLong, D. N. Fittinghoff, J. N. Sweetser, M. A. Krumbügel, B. A. Richman, and D. J. Kane, Rev. Sci. Instrum. **68**, 3277 (1997).
[30] M. Chergui, Low Temp. Phys. **26**, 632 (2000).
[31] G. P. Zhang and T. F. George, Phys. Rev. Lett. **93**, 147401 (2004).
[32] A. Reinköster, S. Korica, G. Prümper, J. Viefhaus, K. Godehusen, O. Schwarzkopf, M. Mast, and U. Becker, J. Phys. B **37**, 2135 (2004).
[33] P. N. Juranic, D. Lukic, K. Barger, and R. Wehlitz, Phys. Rev. A **73**, 042701 (2006).
[34] S. Matt, D. Muigg, A. Ding, C. Lifshitz, P. Scheier, and T. D. Märk, J. Phys. Chem. **100**, 8692 (1996).
[35] C. Lifshitz, Int. J. Mass Spectrom. **198**, 1 (2000).

[36] I. V. Hertel and C. P. Schulz, *Atome, Moleküle und Optische Physik* (Springer, Berlin, Heidelberg, 2008), Vol. 1.

[37] We estimate the resonant dynamic Stark effect, equivalent to the Autler–Townes or Rabi splitting (see, e.g., Ref. 36) as $e_0 r_{ab} E_0$ with the transition dipole moment $e_0 r_{ab}$ from the measured oscillator strength $f=0.015$ for "feature a" of Ref. 25 at 3.05 eV and the electric field strength $E_0/(\mathrm{V/m}) = 2745\sqrt{I_0/(\mathrm{W/cm^2})}$ at our present intensities $I_0 = 3.4 \times 10^{13}$ W/cm^2 to be $\simeq 100$ meV—which is larger than most of the vibrational level splittings in C_{60}.

[38] Assuming that the total energy of the system is—after a few picoseconds—statistically distributed over the vibrational degrees of freedom, the kinetic shift energy is required to allow for channeling the necessary dissociation energy with sufficient probability into the coordinates involved in the bond breaking.

[39] Note that for higher charge states an even faster relaxation would be expected. These ions, however, cannot be detected here due to the relatively weak probe pulse.